



1 **Impact of Western Pacific Subtropical High on Ozone**
2 **Pollution over Eastern China**

3 **Zhongjing Jiang¹, Jing Li¹, Xiao Lu², Cheng Gong³, Lin Zhang¹, Hong Liao⁴**

4

5 1 Department of Atmospheric and Oceanic Sciences, School of Physics, Peking
6 University, Beijing, China

7 2 School of Engineering and Applied Sciences, Harvard University, Cambridge, USA

8 3 Institute of Atmospheric Physics, Chinese Academy of Sciences, Beijing, China

9 4 Jiangsu Key Laboratory of Atmospheric Environment Monitoring and Pollution
10 Control, Jiangsu Collaborative Innovation Center of Atmospheric Environment and
11 Equipment Technology, School of Environmental Science and Engineering, Nanjing
12 University of Information Science and Technology, Nanjing, China

13

14 †Corresponding author: jing-li@pku.edu.cn

15

16

17 **Abstract**

18 Surface ozone is a major pollutant in Eastern China, especially during the summer
19 season. The formation of surface ozone pollution highly depends on meteorological
20 conditions as generally controlled regional circulation patterns. Here we show that
21 summertime ozone pollution over Eastern China is distinctly modulated by the
22 variability of West Pacific Subtropical High (WPSH), a major synoptic system that



23 controls the summertime weather conditions of East Asia. Composite and regression
24 analyses indicate that positive WPSH anomaly is associated with higher than normal
25 surface ozone concentration over Northern China but lower ozone over Southern China.
26 We show that this is mainly driven by changes in meteorological variables with stronger
27 than normal WPSH leading to higher temperatures, stronger solar radiation at the land
28 surface, lower relative humidity, and less precipitation in Northern China, favoring the
29 production and accumulation of surface ozone. In contrast, all variables show reverse
30 changes in Southern China under stronger WPSH. GEOS-Chem simulations reasonably
31 reproduce the observed ozone changes associated with the WPSH and support the
32 statistical analyses. Detailed contributions of different processes are quantified through
33 budget diagnosis, which emphasizes the decisive role of chemistry. Natural emission of
34 precursors from biogenic and soil sources accounts for ~30% of the total surface ozone
35 changes.

36

37

38 **Key words:**

39 Surface ozone, WPSH, meteorological fields, GEOS-Chem, precursor

40

41 **1. Introduction**

42

43 Surface ozone is a major trace gas in the lower atmosphere. It is produced by
44 photochemical oxidation of carbon monoxide (CO) and volatile organic compounds



45 (VOCs), in the presence of nitrogen oxides ($\text{NO}_x = \text{NO} + \text{NO}_2$) and sunlight. Not only
46 does it act as a greenhouse gas but it also exerts detrimental effects on both human
47 health and the ecosystem (Heck et al., 1983; Tai et al., 2014; Monks et al., 2015; Liu et
48 al., 2018; Maji et al., 2019). In China, the problem of tropospheric ozone pollution is
49 severe in most urban areas, such as the North China Plain (NCP), the Yangtze River
50 Deltas (YRD), and Pearl River Deltas (PRD) (Li et al., 2019; Lu et al., 2018; Silver et
51 al., 2018; Yin et al., 2019). Typically, surface ozone concentration reaches its peak in
52 the summer season due to active photochemistry (Wang et al., 2017; Lu et al., 2018).
53 The summertime daily maximum 8h average (MDA8) ozone concentrations frequently
54 reach or exceed the Grade II national air quality standard of 82 ppbv in NCP (Lu et al.,
55 2018; Ministry of Environmental Protection of the People's Republic of China (MEP),
56 2012). Moreover, recent studies showed that surface ozone concentration has exhibited
57 an increasing trend since 2013 over most parts of China (Li et al., 2019; Lu et al., 2020).
58
59 Surface ozone concentration is distinctly influenced by meteorological conditions,
60 which impact the production, transport, and removal of ozone. For example, solar
61 radiation changes surface ozone via the effects on photolysis rates as well as on biogenic
62 emissions. High temperature tends to enhance ozone pollution through stagnant air
63 masses, thermal decomposition of peroxyacetylnitrate (PAN), and the increase of
64 biogenic emissions (Fehsenfeld et al., 1992; Guenther et al., 2012; Rasmussen et al.,
65 2012). Wind speed is generally anticorrelated with surface ozone, indicating the
66 important role of horizontal wind in pollutant dispersion (Zhang et al., 2015; Gong and



67 Liao, 2019). Moreover, the variabilities of these meteorological variables are not
68 independent but interconnected. The synchronous variation of some meteorological
69 variables can be ascribed to the same synoptic weather pattern, thus increasing efforts
70 have been devoted to identifying the synoptic weather patterns that enhance ozone
71 pollution (Gong and Liao, 2019; Liu et al., 2019; Han et al., 2020). For example, Liu et
72 al. (2019) objectively identified 26 weather types including some led to highly polluted
73 days and proved that synoptic changes account for 39.2% of the interannual increase in
74 the domain-averaged O₃ from 2013 to 2017. Han et al. (2020) also identified six
75 predominant synoptic weather patterns over eastern China in summer to examine the
76 synoptic influence of weather conditions on ozone.

77

78 A dominant system that affects the summertime weather pattern in China is the WPSH.
79 As an essential component of the East Asia summer monsoon, its intensity, shape, and
80 location control the large-scale quasi-stationary frontal zones in East Asia (Huang et al.,
81 2018). WPSH can significantly influence the monsoon circulation, typhoon tracks, and
82 moisture transport (Choi et al., 2019; Gao et al., 2014) and further impact surface ozone
83 in China. Shu et al. (2016) showed stronger WPSH will increase ozone pollution over
84 YRD by enhancing the ozone production as well as trapping the ozone in the boundary
85 layer. Using observations from 2014 to 2016, Zhao et al. (2017) indicated that stronger
86 WPSH in summer leads to a decrease in surface ozone in Southern China but an
87 increase in Northern China through statistical analysis. While these studies arrived at
88 qualitative conclusions, they either focused on a limited region or a short time span, and



89 both lacked a comprehensive investigation of the mechanisms through model
90 simulation. Considering the increasingly severe ozone pollution in China, it is desirable
91 to further investigate this topic systematically.

92

93 For this purpose, this study aims to address how and why summertime surface ozone
94 concentration in Eastern China responds to changes in the WPSH. A joint statistical
95 analysis and model simulation using the GEOS-Chem is performed to reveal their
96 relationship as well as to examine changes in the relevant chemical and physical
97 processes, in order to provide insights into the formation of summertime ozone
98 pollution in China and to shed light on ozone simulation and prediction.

99

100 **2. Data and methods**

101 **2.1. Surface ozone and meteorological data**

102

103 Routine daily monitoring of air quality in China became available since 2013, with the
104 establishment of a national network by the China National Environmental Monitoring
105 Centre. We obtained hourly surface ozone concentration data of all sites available from
106 2014 to 2018 from <https://quotsoft.net/air/>. An *ad hoc* quality control protocol was
107 developed to remove outliers and invalid measurements (see supplementary
108 information and Figure S1 for example of outliers). MDA8 was calculated based on the
109 hourly ozone data. We removed the linear trend of the data and converted the data unit
110 from $\mu\text{g m}^{-3}$ into ppbv for further analysis. The following calculation is done for cities



111 with a longitude greater than 100°E which serves as a boundary for a rough definition
112 of Eastern China.

113

114 Meteorological fields for 2014–2018 was obtained from the Goddard Earth Observing
115 System Forward Processing (GEOS-FP) database, which is the current operational met
116 data product from the Global Modeling and Assimilation Office (GMAO). The data is
117 available at http://ftp.as.harvard.edu/gcgrid/data/GEOS_2x2.5/GEOS_FP. The
118 meteorological variables used include sea level pressure (SLP), cloud cover (CLDTOT),
119 solar radiation (SWGDN), 2m temperature (T2M), 10m U wind (U10M), 10m V wind
120 (V10M), total precipitation (PRECTOT) and relative humidity (RH). These variables
121 are 1-hour averages except for RH that is 3-hour averages. The hourly data is averaged
122 into daily means for further analysis.

123

124 **2.2. WPSH index and composite analysis**

125

126 Figure 1a shows the multi-year averaged summertime SLP field from 1979 to 2018 and
127 Figure 1b shows its standard deviation. Although the center of the high-pressure system
128 is located over the Northeastern Pacific Ocean, it also shows substantial variability over
129 the West Pacific extending to the east coast of China. This west branch has a significant
130 impact on the summer weather patterns over Eastern China. Wang et al. (2013) defined
131 a WPSH index to characterize the change of WPSH intensity. It is calculated as the
132 mean of 850hPa geopotential height anomaly within the 15–25°N and 115–150°E region



133 (red box in Figure 1b), where the maximum interannual variability of WPSH in the
134 Western Pacific Ocean is located. Here we adopted this index to represent the strength
135 and variability of the WPSH.

136

137 Using this WPSH index, we defined three types of WPSH conditions, namely strong,
138 normal, and weak. Specifically, days with WPSH-index exceeding the 90th percentile
139 of its distribution are classified as strong WPSH days, the 45th -55th percentile as normal
140 WPSH days, and those below the 10th percentile as weak WPSH days (Figure 1c).
141 Therefore, each type has 46 days during the summer from 2014 to 2018. Composite
142 analysis of observed and simulated surface ozone, meteorological variable as well as
143 related model processes are performed based on these three types.

144

145

146 **2.3. GEOS-Chem simulations**

147

148 We use the GEOS-Chem chemical transport model (CTM) (Bey et al., 2001; v12.3.2;
149 <http://geos-chem.org>) to verify the responses of surface ozone in Eastern China to
150 changes of the WPSH and to examine changes in the processes involved. GEOS-Chem
151 includes a detailed O_x-NO_x-HC-aerosol-Br mechanism to describe gas and aerosol
152 chemistry (Parella et al., 2012; Mao et al., 2013). The chemical mechanism follows the
153 recommendations by the Jet Propulsion Laboratory (JPL) and the International Union
154 of Pure and Applied Chemistry (IUPAC) (Sander, et al., 2011; IUPAC, 2013).



155 Photolysis rates for tropospheric chemistry are calculated by the Fast-JX scheme (Bian
156 and Prather (2002); Mao et al. (2010)). Transport is computed by the TPCORE
157 advection algorithm of Lin and Rood (1996) with the archived GEOS meteorological
158 data. Cloud convection is computed from the convective mass fluxes in the
159 meteorological archive as described by Wu et al. (2007). As for boundary layer mixing,
160 we used the non-local scheme implemented by Lin and McElroy (2010).

161

162 Emissions are configured using the Harvard-NASA Emission Component (HEMCO)
163 (Keller et al., 2014). Biogenic VOC emissions, including isoprene, monoterpenes, and
164 sesquiterpenes, are calculated online using the Model of Emissions of Gases and
165 Aerosols from Nature (MEGAN v2.1, Guenther et al., 2012). Soil NO_x emissions are
166 calculated based on available nitrogen (N) in soils and edaphic conditions such as soil
167 temperature and moisture (Hudman et al., 2012).

168

169 The model is driven by GEOS-FP meteorology fields and runs with 47 vertical levels
170 and $2^\circ \times 2.5^\circ$ horizontal resolution. The model simulations started from January 1st and
171 ended on August 31st for each year during 2014 to 2018, in which the first 5 months
172 were used as spin-up and June-July-August (JJA) are used for composite analysis.
173 Anthropogenic emissions were fixed in 2010 after which the MIX emission inventory
174 stopped updating, so that the differences among the three types of WPSH are solely
175 caused by the change of meteorology. Because meteorology not only affects the
176 production and transport of ozone but also significantly impacts the emission of BVOCs



177 and NO_x from the soil, two important precursors of ozone formation, we also performed
178 another set of simulations with MEGAN and soil NO_x emissions turned off to explore
179 the contribution of natural emissions. We used ozone levels at the lowest model level
180 with an average height of 58 m to represent model simulated surface ozone
181 concentration.

182

183 **2.4. Ozone Budget diagnosis**

184 The simulated ozone concentration is determined by four processes, namely chemistry,
185 transport (the sum of horizontal and vertical advection), mixing, and convection. Dry
186 deposition is included in mixing since we used the non-local PBL mixing scheme.
187 Budget diagnosis is further performed to quantify their individual contributions. The
188 GEOS-Chem v12.1.0 or later versions provide budget diagnostics defined as the mass
189 tendencies per grid cell (kg s^{-1}) for each species in the column (full, troposphere, or
190 PBL) related to each GEOS-Chem component (e.g, chemistry). These diagnostics are
191 calculated by taking the difference in the vertically integrated column ozone mass
192 before and after chemistry, transport, mixing, and convection component in GEOS-
193 Chem. Here we use the budget diagnostics in the PBL column and calculated composite
194 means for each type of WPSH.

195

196 **3. Results**

197 **3.1. Observed surface ozone changes associated with WPSH intensity**

198



199 We first examine the relationship between observed MDA8 and WPSH-index of all
200 cities in China. Figure 2a&b (symbols) respectively shows the difference in the
201 composite mean of observed MDA8 between strong/weak WPSH days and normal
202 WPSH days. A distinct dipole-like pattern can be observed in Figure 2a, indicating that
203 during strong WPSH events, surface ozone concentration tends to be higher in Northern
204 China but lower in Southern China, especially the southeast region. The transition from
205 positive to negative changes happens around 32°N (Figure 2a), which is then used as
206 the division between Northern and Southern China in this study. In contrast, Figure 2b,
207 which shows the composite mean difference between weak and normal WPSH days,
208 also exhibits a dipole pattern but opposite in sign to that shown in Figure 2a.
209 Quantitatively, for cities with significant differences (p -value<0.05) in Student's t -test,
210 during strong WPSH days, the average MDA8 increased by 10.7 ppbv (+19%, Figure
211 2a&c) in Northern China and decreased by 11.2 ppbv (-24%, Figure 2a&c) in Southern
212 China, Under weak WPSH conditions, the average MDA8 decreased by 10.2 ppbv (-
213 17%, Figure 2b&d) in Northern China and increased by 4.6 ppbv (+10%, Figure 2b&d)
214 in Southern China. This dipole change of ozone is also confirmed by a regression
215 analysis of surface ozone against the WPSH index (Figure 2e), with significant positive
216 signals over Northern China and negative signals in Southern China.

217

218 Composite and regression analysis jointly prove the robustness of the dipole-like ozone
219 anomaly pattern associated with WPSH variability. It is likely that these changes are
220 driven by changes in meteorological conditions. Therefore, in Figure 3, we further



221 examine the differences of major meteorological variables associated with WPSH
222 intensity.

223

224 The change of SLP associated with strong WPSH days clearly shows a positive center
225 in the Northwest Pacific Ocean and to the east of China coast (Figure 3a). This high-
226 pressure center induces anti-cyclonic circulation anomalies, which manifest themselves
227 as southwest wind (10 m) anomalies over Eastern China (Figure 3a). In Northern China,
228 because the surface winds are blown from the land area in the south (Figure 3a), it
229 contains less moisture but with higher temperatures. As a result, Northern China
230 exhibits an increase in temperature (Figure 3k), but decreases in moisture-related
231 variables including precipitation (Figure 3c), relative humidity (Figure 3e), and cloud
232 cover (Figure 3g). The decrease in cloud cover increases the near-surface solar radiation
233 (Figure 3i) and can further change the photochemical reaction rates, which partly
234 explains the increase of ozone concentration (Jeong and Park, 2013; Gong and Liao,
235 2019). The air stagnation associated with higher temperatures, less precipitation may
236 also limit the diffusion and removal of ozone (Lu et al., 2019b; Pu et al., 2017).
237 Moreover, previous studies showed that ozone is negatively correlated with
238 precipitation and RH (Jeong and Park, 2013; Zhang et al., 2015). The overall changes
239 of the meteorological fields in Northern China thus act to enhance surface ozone.

240

241 In Southern China, the south winds bring moisture from the ocean surface, providing
242 ample water vapor for the rain band that forms on the northern boundary of the WPSH



243 (Sampe et al., 2010; Rodriguez et al., 2019). This results in increased precipitation
244 (Figure 3c), relative humidity (Figure 3e), and cloud cover (Figure 3g), and reduced
245 surface shortwave radiation (Figure 3i). The increased precipitation and decreased solar
246 radiation also help to lower the surface temperature (Figure 3k). The corresponding
247 ozone concentration change is thus negative and opposite to that in Northern China. In
248 addition, the transport of ozone-depleted air from the ocean can also dilute surface
249 ozone.

250

251 Under the weak WPSH condition, the high-pressure center in Northwest Pacific is
252 weaker and shifted slightly southward (Figure 3b). The changes of meteorological
253 variables mostly show reversed patterns to those under strong WPSH cases, but some
254 asymmetric features are noticed. For example, solar radiation decreased and total
255 precipitation increased in Guangdong province, which is contrary to the general solar
256 radiation enhancement and precipitation reduction in Southern China. However, these
257 abnormal changes in meteorology well match the observed decrease of ozone in
258 Guangdong province.

259

260 According to the weather anomalies related to WPSH intensity, we summarize two
261 pathways for ozone changes: (1) the relative changes of solar radiation and the
262 associated meteorological variables impacting on the chemical formation of ozone; (2)
263 the transport indicated by wind anomalies serving to enrich or dilute ozone
264 concentration depending on wind direction.



265

266 **3.2. Simulated WPSH impacts on ozone air quality**

267

268 Statistical analysis in Section 3.1 only reveals correlation but not causality. To
269 investigate whether or not the WPSH-related meteorology changes indeed induce the
270 dipole-like ozone change pattern, we perform GEOS-Chem simulations from 2014 to
271 2018 with anthropogenic emissions fixed in 2010. In this way, the model responses are
272 purely attributed to changes in meteorology.

273

274 The model's capability in reproducing the spatial-temporal variability of MDA8
275 concentrations in China is first evaluated by comparing the simulation results from 2014
276 to 2018 over all Chinese cities with observation (Figure S2). GEOS-Chem captures the
277 observed seasonal spatial distributions of MDA8 reasonably well. The spatial
278 correlation coefficients (R) between the observed and simulated seasonal mean MDA8
279 concentrations for summers from 2014 to 2018 are 0.57, 0.59, 0.70, 0.81, and 0.81
280 respectively, proving the reliability of GEOS-Chem to represent the variation of ozone
281 MDA8 concentrations.

282

283 Figure 2 (filled contours) shows the simulated MDA8 changes during strong/weak
284 WPSH days with respect to normal days (a&b) and their relative changes (c&d).
285 Compared with observed changes (symbols), GEOS-Chem model well reproduces the
286 dipole-like pattern of ozone change, albeit with a slight underestimation especially in



287 Northern China. By calculating the average changes of simulated ozone concentration
288 sampled at each city, we find the ozone responses to strong and weak WPSH are quite
289 symmetric, with the average MDA8 increased by 3.6 ppbv (+6%) in Northern China
290 and decreased by 7.1 ppbv (-12%) in Southern China during strong WPSH (Figure 2a),
291 and the average MDA8 decreased by 3.6 ppbv (-6%) in Northern China and increased
292 by 6.6 ppbv (+11%) in Southern China during weak WPSH (Figure 2b). The slight
293 underestimation of model results may come from the model's lack of ability in
294 capturing the peak values of ozone MDA8 (Zhang and Wang, 2016; Ni et al, 2018).

295

296 **3.3 Budget diagnosis**

297

298 In order to examine and to quantify the chemical and physical processes that lead to the
299 ozone change, Figure 4 provides the budget diagnostics of chemistry, transport, mixing,
300 and convection in the PBL column. Chemistry represents the changes in net chemical
301 production, which is determined by the change of reaction rate and the amount of ozone
302 precursors. As the photolysis rate and natural precursor emissions are both influenced
303 by meteorological conditions, the change of chemical production is consistent with the
304 variation of solar radiation and temperature in Figure 3. Under the strong WPSH
305 condition, ozone concentrations from chemical production exhibit a tripolar structure,
306 with increases in Northern China and the southern edge and decreases in the Yangtze
307 River basin (Figure 4a).

308



309 Transport represents the change of horizontal and vertical advection of ozone. As wind
310 anomalies associated with strong WPSH (Figure 3a) tend to dilute surface ozone in the
311 south and accumulate ozone in the north, the resulting ozone change exhibits an
312 asymmetric pattern with decreases in most of Southern China and increases over
313 Northern and Northeastern China. The mixing process describes the turbulence
314 diffusion in the boundary layer. Mixing in the whole PBL column represents the total
315 exchange of PBL with the free atmosphere, which shows a roughly reversed pattern to
316 chemistry (Figure 4e). Cloud convection shows a general dipole pattern with positive
317 signals in the north and negative signals in the south. However, the small changes in the
318 absolute value suggest a weak impact via deep convection (Figure 4g). Under weak
319 WPSH conditions, ozone from chemical production significantly increases in the east
320 of Southern China but decreases strongly in Northern and Southwestern China (Figure
321 4b). According to the wind anomalies in Figure 3b, transport tends to minimize the
322 difference induced by chemistry and thus leads to an opposite ozone change (Figure
323 4d). Mixing shows a distinct north-south contrast pattern (Figure 4f). Convection
324 changes slightly in opposite direction in the north and south (Figure 4h). Due to PBL
325 mixing, the total change of these processes (Figure 4i&j) in the PBL column shows a
326 consistent pattern with both the observed and simulated change of surface ozone (Figure
327 2). In general, chemistry (Figure 4a&b) and transport (Figure 4c&d) account for the
328 largest proportions of ozone change than the other two mechanisms (i.e., mixing, Figure
329 4e&f, and convection, Figure 4g&h).

330



331 In order to provide a more quantitative evaluation of the contribution of these processes,
332 in Figure 4k-n, we examine the regionally averaged ozone changes for a North (36.0-
333 42.0°N, 105.0-117.5°E) and South (26.0-32.0°N, 107.5-120.0°E) region, respectively
334 defined by the purple and black boxes on Figure 4i&j. It can be seen that the regionally
335 averaged total ozone change is around $\pm 1-2 \text{ kg s}^{-1}$. In all cases except Northern China
336 under strong WPSH, chemistry appears to be the dominating process, which results in
337 the largest ozone change and with the same sign as the total change and sometimes can
338 even exceed the amount of total change. For the Northern China case, transport slightly
339 outweighs chemistry as the primary factor (Figure 4k). Transport contributes to total
340 changes either positively or negatively, depending on the ozone concentration gradient
341 and wind anomalies. It tends to increase ozone when the wind anomalies come from
342 inland regardless of the direction (Figure 4k&m&n). In contrast, when the wind comes
343 from the ocean, it serves to reduce surface ozone (Figure 4l). As the mixing process
344 transports ozone along the vertical concentration gradient, it generally contributes
345 negatively to the total ozone change and thus counteracts excessive chemical changes
346 (Figure 4l-n). Convection only induces minor modulation to the total changes, generally
347 less than $\pm 1 \text{ kg s}^{-1}$ and negligible for some cases (Figure 4l&m).

348

349 **3.4 The contribution of natural emission of ozone precursor gases**

350

351 In the GEOS-Chem simulation, all anthropogenic emissions are fixed so there is no
352 anthropogenic contribution to the simulated ozone change. However, the emission of



353 ozone precursor gases from natural sources, primarily biogenic volatile organic
354 compounds (BVOCs) and soil-released NO_x (SNO_x), closely respond to meteorology
355 and further impact the chemical production of ozone which has been identified as the
356 main driving force of ozone change. Therefore, in this section, we continue to quantify
357 the contribution of BVOCs and soil NO_x emission to the ozone changes with WPSH.

358

359 Isoprene (used as a proxy of BVOCs) emissions are strongly correlated with
360 temperatures and increase rapidly between 15 and 35 °C (Fehsenfeld et al., 1992;
361 Guenther et al., 1993), thus the pattern of their changes with WPSH are highly
362 consistent with the T₂ changes (Figure 5a&b). Intensified WPSH results in 10-40%
363 increases of BVOCs emissions in Northern China and 10-30% decreases in Southern
364 China, whereas under weak WPSH conditions, they increase strongly in most parts of
365 China but with a slight decrease over the Northern China Plain and Northeastern China.
366 Changes of NO_x emission from the soil also exhibit a similar pattern to those of T₂.
367 Their responses to weak WPSH appear to be stronger than BVOCs, with decreases up
368 to 40% over most of Northern China (Figure 5c&d). As most parts of China are the
369 high-NO_x and VOC-limited regions, the overall decreases of BVOCs and NO_x reduce
370 the ozone concentration.

371

372 We further quantify the contribution of BVOCs and soil NO_x emissions to the changes
373 in surface ozone concentration, by comparing simulation results with MEGAN and soil
374 emissions turned on and off. Figure 6a&b and 6c&d shows the simulated MDA8 ozone



375 with biogenic and soil NO_x emissions on and off respectively. They show similar spatial
376 patterns but the emission-off case exhibits weaker responses. Figure 6e&f shows their
377 differences, which represent the MDA8 changes due to the combined effect of BVOCs
378 and soil NO_x emission changes associated with WPSH variation. The precursor-
379 induced ozone changes are in phase with the total ozone changes in most parts of China
380 and show a dipole-like pattern. In total, these two factors result in $\sim\pm 1.3$ ppbv MDA8
381 ozone changes (averaged over all cities), which accounts for around 30% of the total
382 simulated change. Figure 6g&h and i&j show the contribution of soil NO_x and BVOCs
383 emissions respectively, from which we can see that the ozone change induced by soil
384 NO_x is weaker, implying that BVOCs is the dominant factor. Figure 6k-n shows the
385 averaged contributions from individual and total emissions of BVOCs and soil NO_x for
386 a north and south region marked respectively by purple and black boxes in Figure 6a&b.
387 The averaged ozone changes in the North and South region are in the range of -4-4
388 ppbv, and BVOCs and soil NO_x on average contribute 28% to the total changes. The
389 combined contribution of BVOCs and soil NO_x is more consistent with that of BVOCs,
390 and the soil NO_x-induced changes are small in all cases except Northern China under
391 the weak WPSH conditions. The exception in Figure 6m might be due to the ratio of
392 VOC to NO_x in the North region under weak WPSH conditions, which shifts towards
393 the NO_x-limited regime, making ozone concentration more sensitive to the change of
394 NO_x. In sum, the result emphasizes the role of BVOCs emission in total chemistry
395 production.
396



397

398 **4. Conclusions and Discussion**

399

400 In this study, we highlight the role of weather systems like WPSH on surface ozone
401 pollution in China interpreted with a comprehensive mechanism analysis. Statistical
402 analysis of surface observation reveals a dipole-like ozone change associated with the
403 WPSH intensity, with stronger WPSH increasing surface ozone concentration over
404 Northern China but reducing it over Southern China, and a reversed pattern during its
405 weak phase. This phenomenon is associated with the change of meteorological
406 conditions induced by the change of WPSH intensity. Specifically, when WPSH is
407 stronger than normal, dry, hot south winds from inland area serves to increase
408 temperature in Northern China but decrease relative humidity, cloud cover, and
409 precipitation, creating an environment that is favorable for surface ozone formation. In
410 Southern China, the south winds transport ozone-poor air as well as water vapor from
411 the ocean, which dilute ozone and also increase relative humidity, cloud cover, and
412 precipitation, and decreases solar radiation. Opposite changes are found during weaker
413 WPSH conditions.

414

415 This dipole pattern of surface ozone changes is well reproduced by the GEOS-Chem
416 model simulations. Diagnosing the model budgets also suggests that chemistry serves
417 as the key process determining the direction of the ozone change, including both
418 changes in BVOCs and soil NO_x emissions and the changes in chemical reaction rates



419 with the WPSH intensity. Ozone changes caused by natural emission (including BVOCs
420 and soil NO_x) accounts for ~30% of the total ozone changes.

421

422 As WPSH is associated with continental scale circulation patterns, such as the East
423 Asian Summer Monsoon (EASM), several previous studies also discussed the impact
424 of EASM on ozone pollution in China (Yang et al., 2014; Han et al., 2020). However,
425 our study differs from the EASM related ones in that (1) the EASM has complex space
426 and time structures that encompass tropics, subtropics, and midlatitudes. Given its
427 complexity, it is difficult to use a simple index to represent the variability of EASM
428 (Wang et al., 2008; Ye et al., 2019), whereas the location and definition for WPSH are
429 much definitive (Lu et al., 2002; Wang et al., 2012); and (2) The influences of EASM
430 on ozone mainly represent interannual scale as EASM indices are defined by
431 month/year, while the WPSH is a system more suitable to explore the day to day
432 variability ozone, which is meaningful for short-term ozone air quality prediction.

433

434 A better understanding of the internal mechanism of WPSH's impact on ozone air
435 quality can also help assess the air quality variation more comprehensively under
436 climate change. The location and intensity of WPSH keep changing over time, e.g.,
437 Zhou et al. (2009) demonstrated that WPSH has extended westward since the late 1970s,
438 and Li et al. (2012) indicated that North Pacific Subtropical High will intensify in the
439 twenty-first century as climate warms. Nonetheless, there still exists a great uncertainty
440 about how WPSH will change under climate change, and further studies are needed to



441 discuss the responses of ozone to synoptic weather systems like WPSH in future
442 scenarios. In addition, the variability of WPSH is found to be related to global climate
443 variabilities such as ENSO (Paek et al., 2019) and PDO (Matsumura et al., 2016).
444 Therefore, how natural climate variabilities like ENSO and PDO interact with WPSH
445 to impact ozone air quality also needs more investigation.

446

447 **Data and model availability**

448 All the measurements, meteorological data are accessible online through the websites
449 given above. The GEOS-Chem model is a community model and is freely available
450 (www.geos-chem.org).

451

452 **Author contributions**

453 J.L. and Z.J. designed the study. Z.J. ran the GEOS-Chem model and performed the
454 analysis. X.L. and L.Z. helped in the GEOS-Chem simulation. C.G. and H.L. helped in
455 the budget diagnosis. Z.J. and J.L. wrote the paper. All authors contributed to the
456 interpretation of results and the improvement of this paper.

457

458 **Competing interests**

459 The authors declare that they have no conflict of interest.

460

461 **Acknowledgement**

462 We thank the China National Environmental Monitoring Centre for supporting the



463 nationwide ozone monitoring network and the website (<http://beijingair.sinaapp.com/>)
464 for collecting and sharing hourly ozone concentration data. We appreciate GMAO for
465 providing the GEOS-FP meteorological data
466 (http://ftp.as.harvard.edu/gcgrid/data/GEOS_2x2.5/GEOS_FP). We also acknowledge
467 the efforts of GEOS-Chem Working Groups and Support Team for developing and
468 maintaining the GEOS-Chem model.

469

470 **Financial Support**

471 This work is funded by the National Key Research and Development Program of China
472 (No. 2017YFC0212803) and Open fund by Jiangsu Key Laboratory of Atmospheric
473 Environment Monitoring and Pollution Control (KHK1901).

474

475 **References**

476 Bey, I., Jacob, D. J., Yantosca, R. M., Logan, J. A., Field, B. D., Fiore, A. M., Li, Q.,
477 Liu, H. Y., Mickley, L. J., and Schultz, M. G.: Global modeling of tropospheric
478 chemistry with assimilated meteorology: Model description and evaluation, *J.*
479 *Geophys. Res.*, 106, 23073-23095, <https://doi.org/10.1029/2001JD000807>, 2001.
480 Bian, H. S., and Prather, M. J.: Fast-J2: Accurate simulation of stratospheric photolysis
481 in global chemical models, *J. Atmos. Chem.*, 41, 281-296,
482 <https://doi.org/10.1023/a:1014980619462>, 2002.
483 Choi, W., and Kim, K.-Y.: Summertime variability of the western North Pacific
484 subtropical high and its synoptic influences on the East Asian weather, *Sci. Rep.*, 9,



- 485 <https://doi.org/10.1038/s41598-019-44414-w>, 2019.
- 486 Fehsenfeld, F., Calvert, J., Fall, R., Goldan, P., Guenther, A., Hewitt, C., Lamb, B., Liu,
487 S., Trainer, M., Westberg, H., and Zimmerman, P.: Emissions of volatile organic
488 compounds from vegetation and the implications for atmospheric chemistry, *Global*
489 *Biogeochem. Cycles*, 6, 389-430, <https://doi.org/10.1029/92gb02125>, 1992.
- 490 Gao, H., Jiang, W., and Li, W.: Changed Relationships Between the East Asian Summer
491 Monsoon Circulations and the Summer Rainfall in Eastern China, *J. Meteorolog.*
492 *Res.*, 28, 1075-1084, <https://doi.org/10.1007/s13351-014-4327-5>, 2014.
- 493 Gong, C., and Liao, H.: A typical weather pattern for ozone pollution events in North
494 China, *Atmos. Chem. Phys.*, 19, 13725-13740, [https://doi.org/10.5194/acp-19-](https://doi.org/10.5194/acp-19-13725-2019)
495 13725-2019, 2019.
- 496 Guenther, A. B., Zimmerman, P. R., Harley, P. C., Monson, R. K., and Fall, R.: Isoprene
497 and monoterpene emission rate variability, Model evaluations and sensitivity
498 analyses, *J. Geophys. Res.*, 98, 12609-12617, <https://doi.org/10.1029/93jd00527>,
499 1993.
- 500 Guenther, A. B., Jiang, X., Heald, C. L., Sakulyanontvittaya, T., Duhl, T., Emmons, L.
501 K., and Wang, X.: The Model of Emissions of Gases and Aerosols from Nature version
502 2.1 (MEGAN2.1): an extended and updated framework for modeling biogenic emis-
503 sions, *Geosci. Model Dev.*, 5, 1471-1492, [https://doi.org/10.5194/gmd-5-](https://doi.org/10.5194/gmd-5-1471-2012) 1471-2012,
504 2012.
- 505 Han, H., Liu, J., Shu, L., Wang, T., and Yuan, H.: Local and synoptic meteorological
506 influences on daily variability in summertime surface ozone in eastern China, *Atmos.*



- 507 Chem. Phys., 20, 203-222, <https://doi.org/10.5194/acp-20-203-2020>, 2020.
- 508 Heck, W. W., Adams, R. M., Cure, W. W., Heagle, A. S., Heggstad, H. E., Kohut, R.
509 J., Kress, L. W., Rawlings, J. O., and Taylor, O. C.: A reassessment of crop loss from
510 ozone, Environ. Sci. Technol., 17, A572-A581, <https://doi.org/10.1021/es00118a001>,
511 1983.
- 512 Hoesly, R. M., Smith, S. J., Feng, L., Klimont, Z., Janssens-Maenhout, G., Pitkanen, T.,
513 Seibert, J. J., Linh, V., Andres, R. J., Bolt, R. M., Bond, T. C., Dawidowski, L.,
514 Kholod, N., Kurokawa, J.-i., Li, M., Liu, L., Lu, Z., Moura, M. C. P., O'Rourke, P.
515 R., and Zhang, Q.: Historical (1750-2014) anthropogenic emissions of reactive gases
516 and aerosols from the Community Emissions Data System (CEDS), Geosci. Model
517 Dev., 11, 369-408, <https://doi.org/10.5194/gmd-11-369-2018>, 2018.
- 518 Huang, Y., Wang, B., Li, X., and Wang, H.: Changes in the influence of the western
519 Pacific subtropical high on Asian summer monsoon rainfall in the late 1990s, Clim.
520 Dyn., 51, 443-455, <https://doi.org/10.1007/s00382-017-3933-1>, 2018.
- 521 Hudman, R. C., Moore, N. E., Mebust, A. K., Martin, R. V., Russell, A. R., Valin, L.
522 C., and Cohen, R. C.: Steps towards a mechanistic model of global soil nitric oxide
523 emissions: implementation and space based-constraints, Atmos. Chem. Phys., 12,
524 7779-7795, <https://doi.org/10.5194/acp-12-7779-2012>, 2012.
- 525 IUPAC: Task group on atmospheric chemical kinetic data evaluation by International
526 Union of Pure and Applied Chemistry (IUPAC), available at: [http://iupac.pole-](http://iupac.pole-ether.fr/)
527 [ether.fr/](http://iupac.pole-ether.fr/) (last access: 12th May 2020), 2013.
- 528 Jacob, D. J., and Winner, D. A.: Effect of climate change on air quality, Atmos.



- 529 Environ., 43, 51-63, <https://doi.org/10.1016/j.atmosenv.2008.09.051>, 2009.
- 530 Jeong, J. I. and Park, R. J.: Effects of the meteorological variability on regional air
531 quality in East Asia, Atmos. Environ., 69, 46–55,
532 <https://doi.org/10.1016/j.atmosenv.2012.11.061>, 2013.
- 533 Keller, C. A., Long, M. S., Yantosca, R. M., Da Silva, A. M., Pawson, S., and Jacob,
534 D. J.: HEMCO v1.0: a versatile, ESMF-compliant component for calculating
535 emissions in atmospheric models, Geosci. Model Dev., 7, 1409–1417,
536 <https://doi.org/10.5194/gmd-7-1409-2014>, 2014.
- 537 Kuhns, H., Knipping, E. M., and Vukovich, J. M.: Development of a United States–
538 Mexico Emissions Inventory for the Big Bend Regional Aerosol and Visibility
539 Observational (BRAVO) Study, J. Air Waste Manage. Assoc., 55, 677-692,
540 <https://doi.org/10.1080/10473289.2005.10464648>, 2005.
- 541 Li, K., Jacob, D. J., Liao, H., Shen, L., Zhang, Q., and Bates, K. H.: Anthropogenic
542 drivers of 2013-2017 trends in summer surface ozone in China, PNAS, 116, 422-427,
543 <https://doi.org/10.1073/pnas.1812168116>, 2019.
- 544 Li, M., Zhang, Q., Kurokawa, J.-i., Woo, J.-H., He, K., Lu, Z., Ohara, T., Song, Y.,
545 Streets, D. G., Carmichael, G. R., Cheng, Y., Hong, C., Huo, H., Jiang, X., Kang, S.,
546 Liu, F., Su, H., and Zheng, B.: MIX: a mosaic Asian anthropogenic emission inventory
547 under the international collaboration framework of the MICS-Asia and HTAP, Atmos.
548 Chem. Phys., 17, 935-963, <https://doi.org/10.5194/acp-17-935-2017>, 2017a.
- 549 Li, W., Li, L., Ting, M., and Liu, Y.: Intensification of Northern Hemisphere subtropical
550 highs in a warming climate, Nat. Geosci., 5, 830-834,



- 551 <https://doi.org/10.1038/ngeo1590>, 2012.
- 552 Lin, J.-T., and M. McElroy, Impacts of boundary layer mixing on pollutant vertical
553 profiles in the lower troposphere: Implications to satellite remote sensing, *Atmos.*
554 *Environ.*, 44(14), 1726-1739, <https://doi.org/10.1016/j.atmosenv.2010.02.009>, 2010.
- 555 Lin, S., and Rood, R. B.: Multidimensional Flux-Form Semi-Lagrangian Transport
556 Schemes, *Mon. Weather Rev.*, 124, 2046-2070, 10.1175/1520-
557 0493(1996)124<2046:MFFSLT>2.0.CO;2, 1996.
- 558 Liu, H., Liu, S., Xue, B., Lv, Z., Meng, Z., Yang, X., Xue, T., Yu, Q., and He, K.:
559 Ground-level ozone pollution and its health impacts in China, *Atmos. Environ.*, 173,
560 223-230, <https://doi.org/10.1016/j.atmosenv.2017.11.014>, 2018.
- 561 Liu, J., Wang, L., Li, M., Liao, Z., Sun, Y., Song, T., Gao, W., Wang, Y., Li, Y., Ji, D.,
562 Hu, B., Kerminen, V.-M., Wang, Y., and Kulmala, M.: Quantifying the impact of
563 synoptic circulation patterns on ozone variability in northern China from April to
564 October 2013-2017, *Atmos. Chem. Phys.*, 19, 14477-14492,
565 <https://doi.org/10.5194/acp-19-14477-2019>, 2019.
- 566 Lu, R.: Indices of the summertime western North Pacific subtropical high, *Adv. Atmos.*
567 *Sci.*, 19, 1004-1028, <https://doi.org/10.1007/s00376-002-0061-5>, 2002.
- 568 Lu, X., Hong, J., Zhang, L., Cooper, O. R., Schultz, M. G., Xu, X., Wang, T., Gao, M.,
569 Zhao, Y., and Zhang, Y.: Severe Surface Ozone Pollution in China: A Global
570 Perspective, *Environ. Sci. Technol. Lett.*, 5, 487-494,
571 <https://doi.org/10.1021/acs.estlett.8b00366>, 2018.
- 572 Lu, X., Zhang, L., and Shen, L.: Meteorology and Climate Influences on Tropospheric



573 Ozone: a Review of Natural Sources, Chemistry, and Transport Patterns, Current
574 Pollution Reports, 5, 238-260, <https://doi.org/10.1007/s40726-019-00118-3>, 2019a.

575 Lu, X., Zhang, L., Chen, Y., Zhou, M., Zheng, B., Li, K., Liu, Y., Lin, J., Fu, T.-M.,
576 and Zhang, Q.: Exploring 2016-2017 surface ozone pollution over China: source
577 contributions and meteorological influences, Atmos. Chem. Phys., 19, 8339-8361,
578 <https://doi.org/10.5194/acp-19-8339-2019>, 2019b.

579 Lu, X., Zhang, L., Wang, X., Gao, M., Li, K., Zhang, Y., Yue, X., and Zhang, Y.: Rapid
580 increases in warm-season surface ozone and resulting health impact over China since
581 2013, Environ. Sci. Technol. Lett., <https://doi.org/10.1021/acs.estlett.0c00171>, 2020.

582 Maji, K. J., Ye, W.-F., Arora, M., and Nagendra, S. M. S.: Ozone pollution in Chinese
583 cities: Assessment of seasonal variation, health effects and economic burden, Environ.
584 Pollut., 247, 792-801, <https://doi.org/10.1016/j.envpol.2019.01.049>, 2019.

585 Mao, J., Sun, Z., and Wu, G.: 20–50-day oscillation of summer Yangtze rainfall in
586 response to intraseasonal variations in the subtropical high over the western North
587 Pacific and South China Sea, Clim. Dyn., 34, 747-761,
588 <https://doi.org/10.1007/s00382-009-0628-2>, 2010.

589 Mao, J., Paulot, F., Jacob, D. J., Cohen, R. C., Crounse, J. D., Wennberg, P. O., Keller,
590 C. A., Hudman, R. C., Barkley, M. P., and Horowitz, L. W.: Ozone and organic
591 nitrates over the eastern United States: Sensitivity to isoprene chemistry, J. Geophys.
592 Res., 118, <https://doi.org/10.1002/jgrd.50817>, 2013.

593 Marais, E. A., and Wiedinmyer, C.: Air Quality Impact of Diffuse and Inefficient
594 Combustion Emissions in Africa (DICE800 Africa), Environ. Sci. Technol., 50,



- 595 10739-10745, <https://doi.org/10.1021/acs.est.6b02602>, 2016.
- 596 Matsumura, S., and Horinouchi, T.: Pacific Ocean decadal forcing of long-term changes
597 in the western Pacific subtropical high, *Sci. Rep.*, **6**, 37765,
598 <https://doi.org/10.1038/srep37765>, 2016.
- 599 Ministry of Environmental Protection of the People's Republic of China, 2012.
600 Ambient Air Quality Standards (GB3095-2012).
- 601 Monks, P. S., Archibald, A. T., Colette, A., Cooper, O. R., Coyle, M., Derwent, R. G.,
602 Fowler, D., Granier, C., Law, K. S., and Mills, G.: Tropospheric ozone and its
603 precursors from the urban to the global scale from air quality to short-lived climate
604 forcer, *Atmos. Chem. Phys.*, **15**, 8889-8973, [https://doi.org/10.5194/acp-15-8889-](https://doi.org/10.5194/acp-15-8889-2015)
605 2015, 2015.
- 606 Ni, R., Lin, J., Yan, Y., and Lin, W.: Foreign and domestic contributions to springtime
607 ozone over China, *Atmos. Chem. Phys.*, **18**, 11447-11469,
608 <https://doi.org/10.5194/acp-18-11447-2018>, 2018.
- 609 Paek, H., Yu, J.-Y., Zheng, F., and Lu, M.-M.: Impacts of ENSO diversity on the
610 western Pacific and North Pacific subtropical highs during boreal summer, *Clim. Dyn.*,
611 **52**, 7153-7172, <https://doi.org/10.1007/s00382-016-3288-z>, 2019.
- 612 Parrella, J. P., Jacob, D. J., Liang, Q., Zhang, Y., Mickley, L. J., Miller, B., Evans, M.
613 J., Yang, X., Pyle, J. A., Theys, N., and Van Roozendaal, M.: Tropospheric bromine
614 chemistry: implications for present and pre-industrial ozone and mercury, *Atmos.*
615 *Chem. Phys.*, **12**, 6723-6740, <https://doi.org/10.5194/acp-12-6723-2012>, 2012.
- 616 Pu, X., Wang, T. J., Huang, X., Melas, D., Zanis, P., Papanastasiou, D. K., and Poupkou,



- 617 A.: Enhanced surface ozone during the heat wave of 2013 in Yangtze River Delta
618 region, China, *Sci. Total Environ.*, 603-604, 807-816,
619 <https://doi.org/10.1016/j.scitotenv.2017.03.056>, 2017.
- 620 Rasmussen, D. J., Fiore, A. M., Naik, V., Horowitz, L. W., McGinnis, S. J., and Schultz,
621 M. G.: Surface ozone-temperature relationships in the eastern US: A monthly
622 climatology for evaluating chemistry-climate models, *Atmos. Environ.*, 47, 142-153,
623 <https://doi.org/10.1016/j.atmosenv.2011.11.021>, 2012.
- 624 Rodriguez, J. M., and Milton, S. F.: East Asian Summer Atmospheric Moisture
625 Transport and Its Response to Interannual Variability of the West Pacific Subtropical
626 High: An Evaluation of the Met Office Unified Model, *Atmosphere*, 10,
627 <https://doi.org/10.3390/atmos10080457>, 2019.
- 628 Sampe, T., and Xie, S.-P.: Large-Scale Dynamics of the Meiyu-Baiu Rainband:
629 Environmental Forcing by the Westerly Jet, *J. Clim.*, 23, 113-134,
630 <https://doi.org/10.1175/2009jcli3128.1>, 2010.
- 631 Sander, S. P., Golden, D., Kurylo, M., Moortgat, G., Wine, P., Ravishankara, A., Kolb,
632 C., Molina, M., Finlayson-Pitts, B., and Huie, R.: Chemical kinetics and
633 photochemical data for use in atmospheric studies, *JPL Publ.*, 06-2, 684 pp., 2011.
- 634 Silver, B., Reddington, C. L., Arnold, S. R., and Spracklen, D. V.: Substantial changes
635 in air pollution across China during 2015–2017, *Environ. Res. Lett.*, 13, 114012,
636 <https://doi.org/10.1088/1748-9326/aae718>, 2018.
- 637 Shu, L., Xie, M., Wang, T., Gao, D., Chen, P., Han, Y., Li, S., Zhuang, B., and Li, M.:
638 Integrated studies of a regional ozone pollution synthetically affected by subtropical



- 639 high and typhoon system in the Yangtze River Delta region, China, *Atmos. Chem.*
640 *Phys.*, 16, 15801-15819, <https://doi.org/10.5194/acp-16-15801-2016>, 2016.
- 641 Tai, A. P. K., Martin, M. V., and Heald, C. L.: Threat to future global food security
642 from climate change and ozone air pollution, *Nat. Clim. Change*, 4, 817-821,
643 <https://doi.org/10.1038/nclimate2317>, 2014.
- 644 van der Werf, G. R., Randerson, J. T., Giglio, L., van Leeuwen, T. T., Chen, Y., Rogers,
645 B. M., Mu, M., van Marle, M. J. E., Morton, D. C., Collatz, G. J., Yokelson, R. J.,
646 and Kasibhatla, P. S.: Global fire emissions estimates during 1997–2016, *Earth Syst.*
647 *Sci. Data*, 9, 697–720, <https://doi.org/10.5194/essd-9-697-2017>, 2017.
- 648 Wang, B., Wu, Z., Li, J., Liu, J., Chang, C.-P., Ding, Y., and Wu, G.: How to Measure
649 the Strength of the East Asian Summer Monsoon, *J. Clim.*, 21, 4449-4463,
650 <https://doi.org/10.1175/2008jcli2183.1>, 2008.
- 651 Wang, B., Xiang, B., and Lee, J.-Y.: Subtropical High predictability establishes a
652 promising way for monsoon and tropical storm predictions, *PNAS*, 110, 2718-2722,
653 <https://doi.org/10.1073/pnas.1214626110>, 2013.
- 654 Wang, T., Xue, L., Brimblecombe, P., Lam, Y. F., Li, L., and Zhang, L.: Ozone
655 pollution in China: A review of concentrations, meteorological influences, chemical
656 precursors, and effects, *Sci. Total Environ.*, 575, 1582-1596,
657 <https://doi.org/10.1016/j.scitotenv.2016.10.081>, 2017.
- 658 Wu, S., L.J. Mickley, D.J. Jacob, J.A. Logan, R.M. Yantosca, and D. Rind, Why are
659 there large differences between models in global budgets of tropospheric ozone?, *J.*
660 *Geophys. Res.*, 112, D05302, <https://doi.org/10.1029/2006JD007801>, 2007.



- 661 Ye, M., and Chen, H.: Recognition of two dominant modes of EASM and its thermal
662 driving factors based on 25 monsoon indexes, *Atmos. Oceanic Sci. Lett.*, 12, 278-
663 285, <https://doi.org/10.1080/16742834.2019.1614424>, 2019.
- 664 Yin, Z., Cao, B., and Wang, H.: Dominant patterns of summer ozone pollution in
665 eastern China and associated atmospheric circulations, *Atmos. Chem. Phys.*, 19,
666 13933–13943, <https://doi.org/10.5194/acp-19-13933-2019>, 2019.
- 667 Zhang, H., Wang, Y., Hu, J., Ying, Q., and Hu, X.-M.: Relationships between
668 meteorological parameters and criteria air pollutants in three megacities in China,
669 *Environ. Res.*, 140, 242-254, <https://doi.org/10.1016/j.envres.2015.04.004>, 2015.
- 670 Zhang, Y. and Wang, Y.: Climate-driven ground-level ozone extreme in the fall over
671 the Southeast United States, *P. Natl. Acad. Sci. USA*, 113, 10025–10030,
672 <https://doi.org/10.1073/pnas.1602563113>, 2016.
- 673 Zhao, Z., and Wang, Y.: Influence of the West Pacific subtropical high on surface ozone
674 daily variability in summertime over eastern China, *Atmos. Environ.*, 170, 197-204,
675 <https://doi.org/10.1016/j.atmosenv.2017.09.024>, 2017.
- 676 Zhou, T., Yu, R., Zhang, J., Drange, H., Cassou, C., Deser, C., Hodson, D. L. R.,
677 Sanchez-Gomez, E., Li, J., Keenlyside, N., Xin, X., and Okumura, Y.: Why the
678 Western Pacific Subtropical High Has Extended Westward since the Late 1970s, *J.*
679 *Clim.*, 22, 2199-2215, <https://doi.org/10.1175/2008jcli2527.1>, 2009.

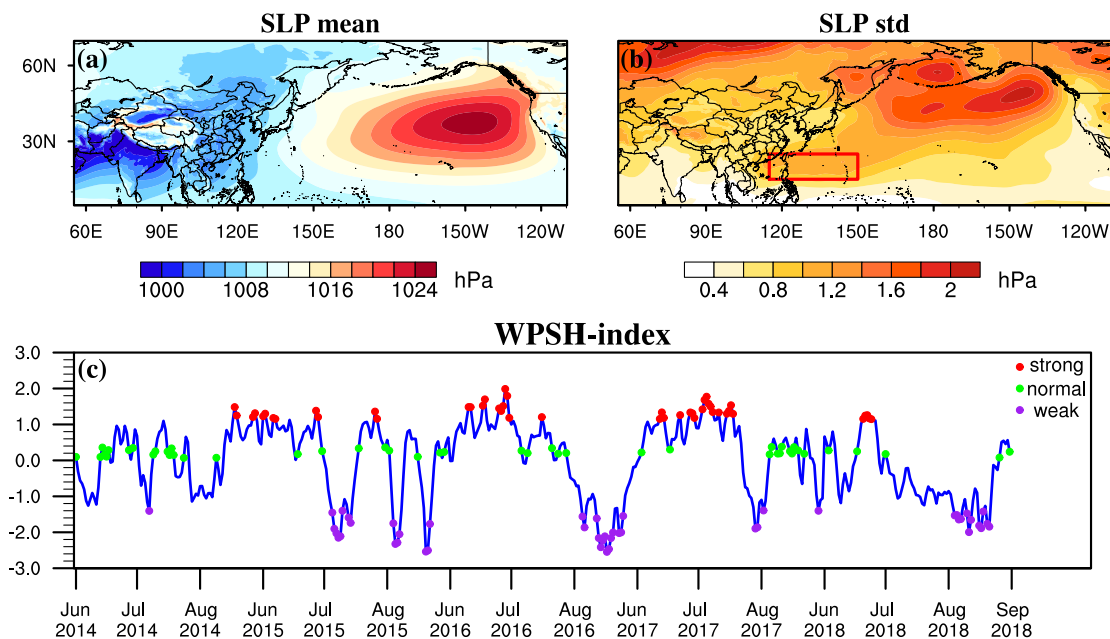


Figure 1. West Pacific Mean Sea Level Pressure (a) and its standard deviation (b), calculated using June, July, August (JJA) data from 1979 to 2018. Red box in (b) indicates the region (15-25°N, 115-150°E) used to calculate the WPSH-index. (c) shows the time series of WPSH-index and the selections of three types of WPSH. The blue line represents the normalized WPSH-index of 460 days in JJA from 2014 to 2018. Red dots represent strong WPSH days, green dots represent normal WPSH days and purple dots represent weak WPSH days.

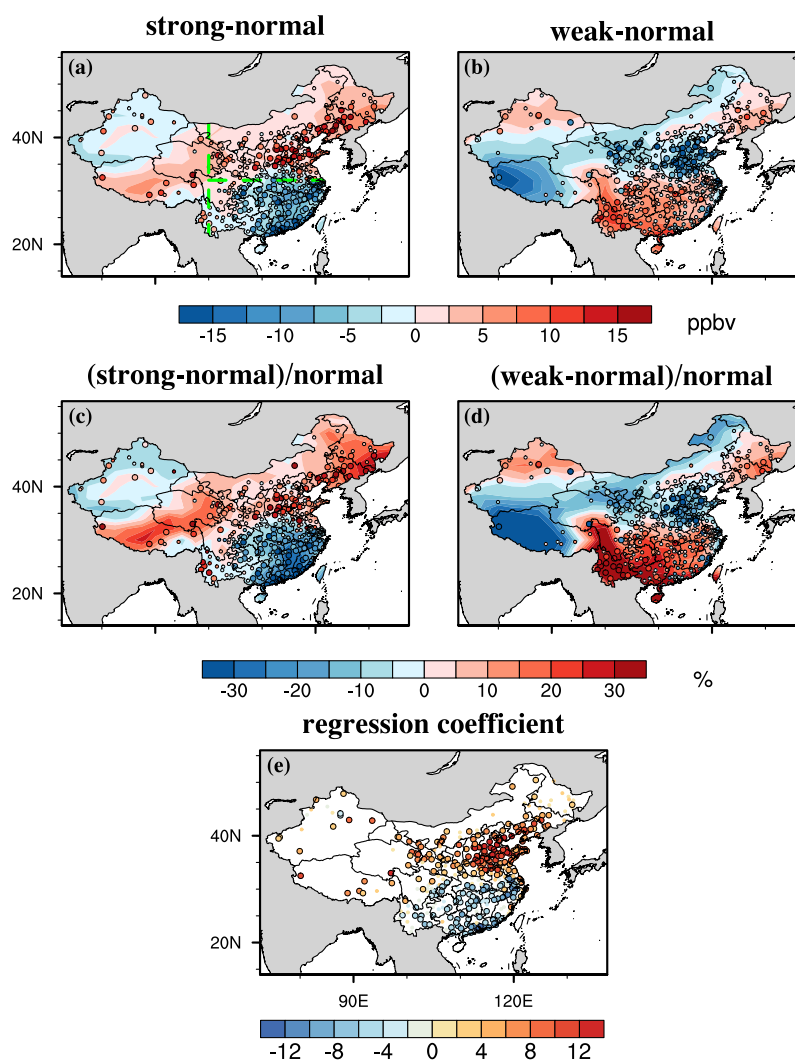


Figure 2. The observed (symbols) and simulated (filled contours) difference of MDA8 (ppbv) during strong and weak WPSH relative to normal WPSH days. (a) MDA8 of strong WPSH minus normal WPSH days, (b) MDA8 of weak WPSH minus normal WPSH days. (c) The percentage change of MDA8 of strong WPSH relative to normal, (d) the percentage change of MDA8 of weak WPSH relative to normal. (e) The regression coefficient between MDA8 in JJA from 2014 to 2018 and WPSH-index for cities in China. Larger dots with black circles in (a-e) are sites with significant level less than 0.05 from Student's *t*-test. The vertical green line in (a) is the boundary of Eastern China and the horizontal green line is the division of Northern and Southern China.

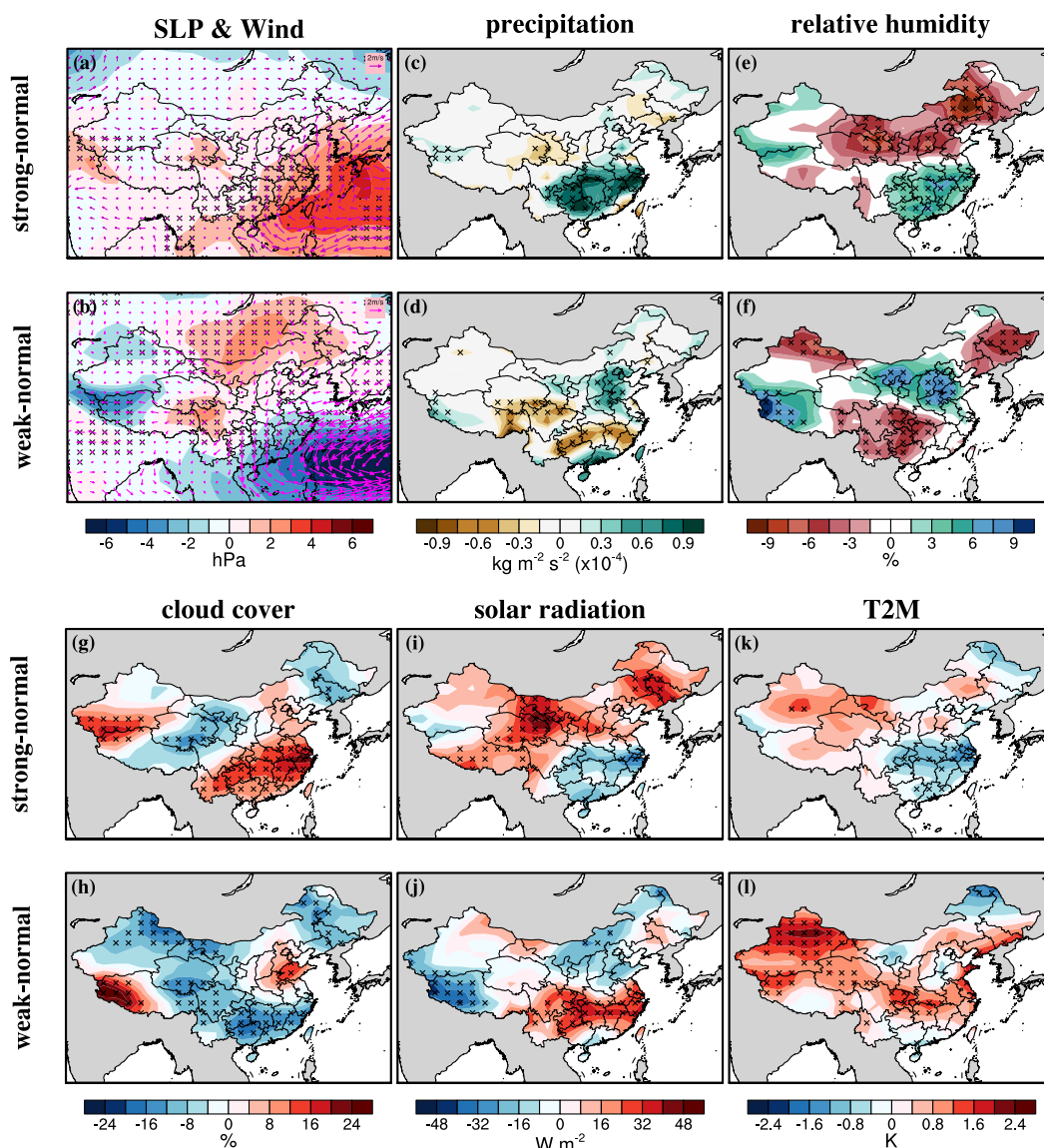


Figure 3. The difference of composite meteorological fields between different WPSH types. The first row corresponds to the difference between strong and normal WPSH days, and the second row correspond to the difference between weak and normal WPSH days. The meteorological variables including SLP, wind, precipitation, relative humidity, cloud cover, solar radiation, and 2 m temperature. The cross symbols indicate grids with significant levels less than 0.05 from Student's *t*-test.

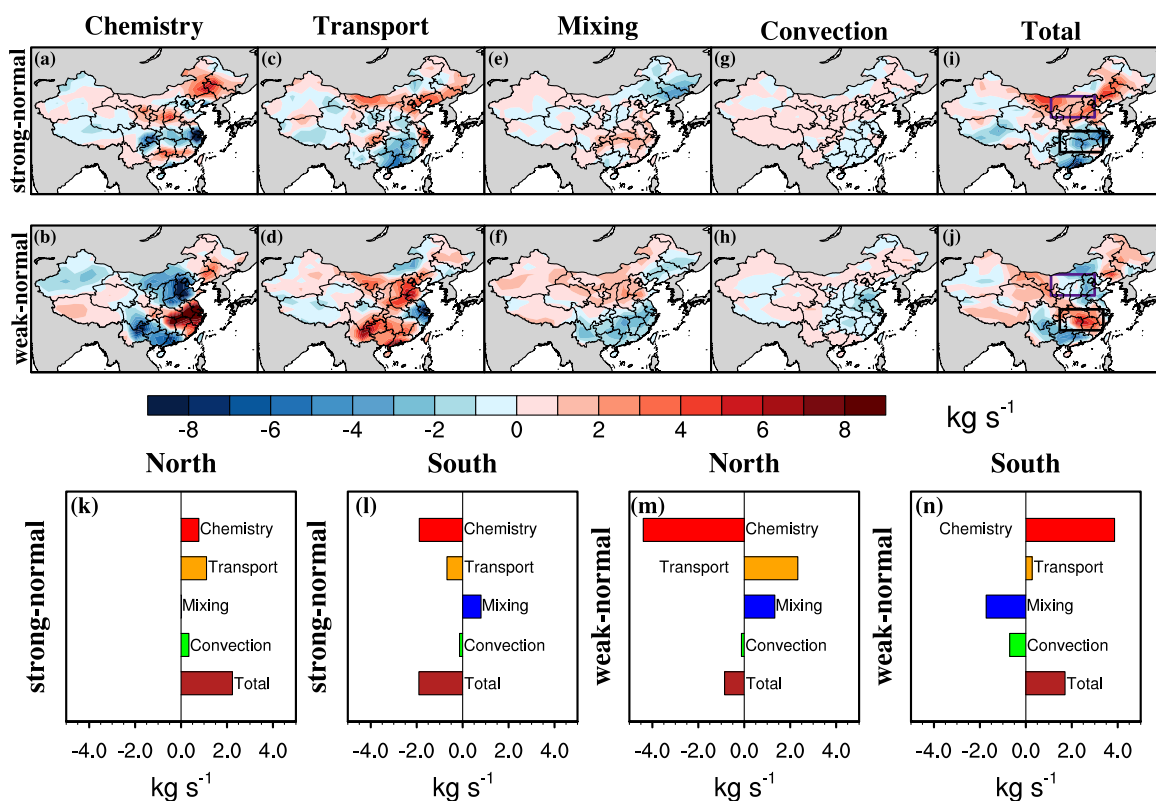


Figure 4. The budget diagnostics (kg s⁻¹) including chemistry, transport, mixing, and convection in the GEOS-Chem model. (a–j) The first row shows the differences between strong and normal WPSH days and the second row shows the differences between weak and normal WPSH days. (k–n) The area-averaged budget diagnostics (kg s⁻¹) for a north (36.0–42.0°N, 105.0–117.5°E) and south (26.0–32.0°N, 107.5–120.0°E) region (purple and black boxes in (i) and (j)).

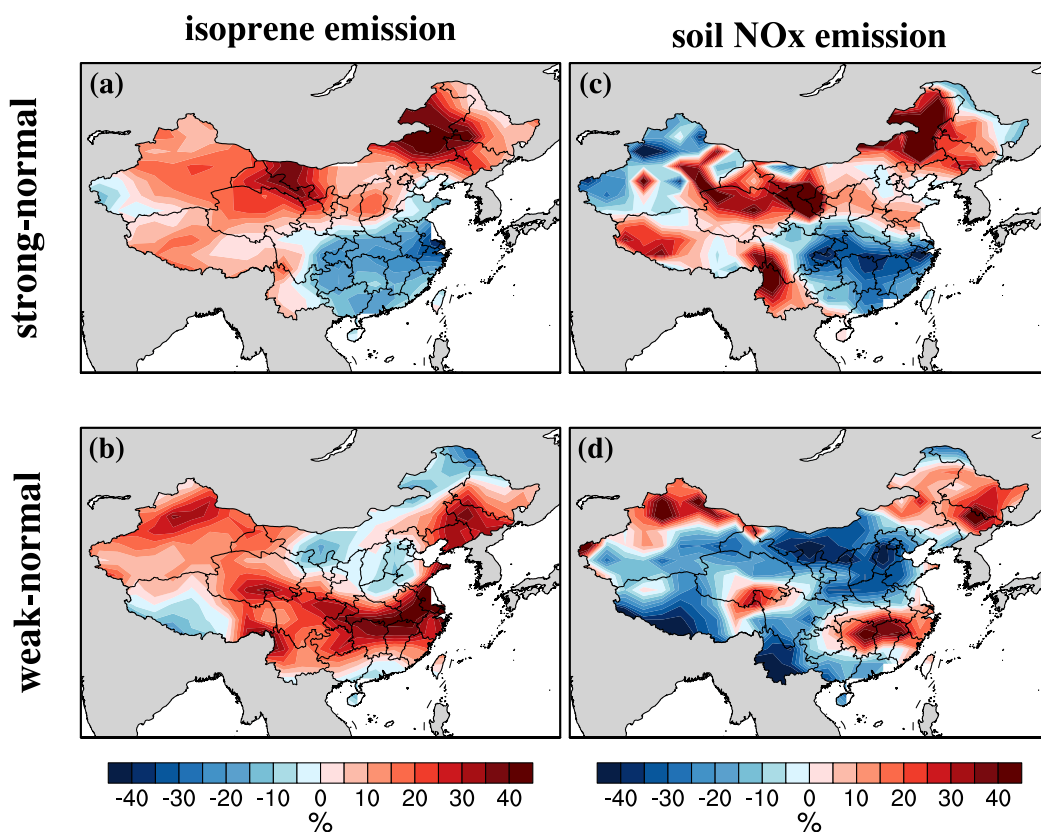


Figure 5. The changes of isoprene (a proxy of biogenic emission), soil NO_x emission in GEOS-Chem model. The first row shows the relative differences (percentage) between strong and normal WPSH conditions and the second row shows those between weak and normal WPSH conditions.

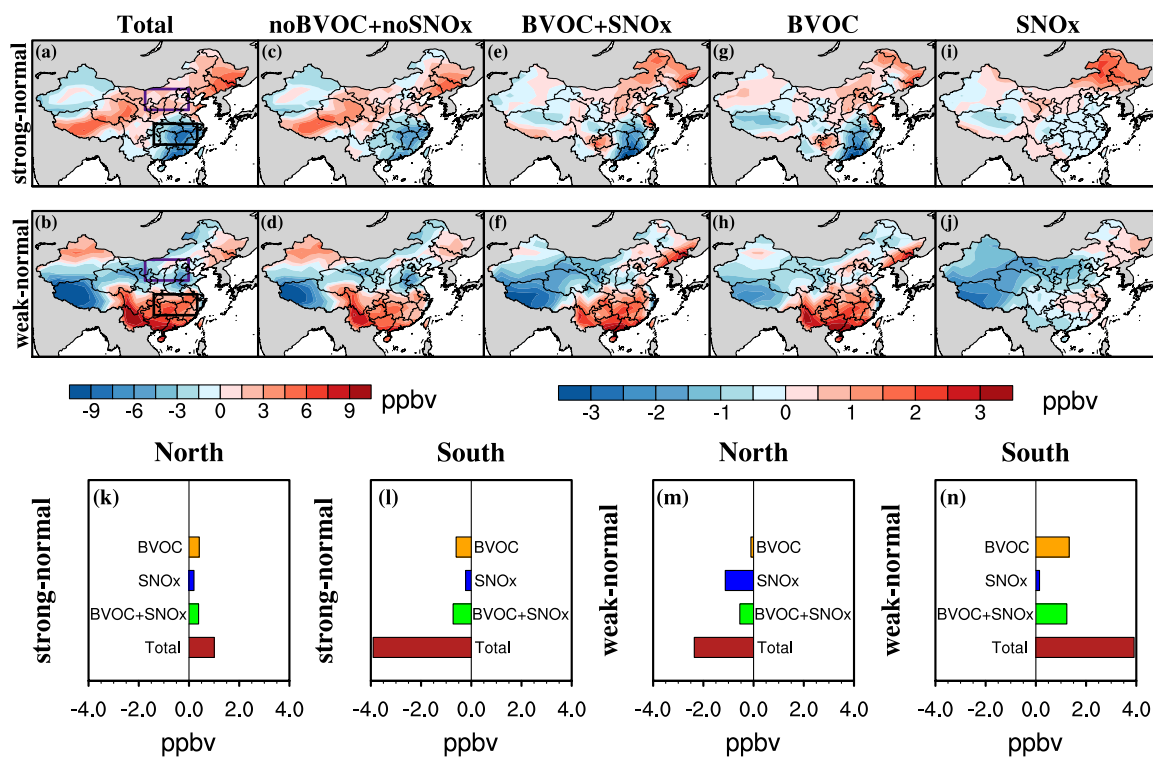


Figure 6. (a) and (b) show the simulated difference of MDA8 (ppbv) of strong and weak WPSH relative to normal WPSH, same as Figure 2a&b (filled contours). (c) and (d) are the same as (a) and (b) except turning off MEGAN and soil NO_x emission. (e) and (f) show the difference between simulations with MEGAN and soil NO_x emission on (Figure 6a&b) and off (Figure 6c&d), which represent the contribution of BVOC and soil NO_x. (g) and (h) show the difference between simulations with MEGAN emission turned on and off, which represent the contribution of BVOC emission. (i) and (j) show the difference between simulations with soil NO_x emission turned on and off, which represent the contribution of soil NO_x emission. Note that (a-d) use the left colorbar and (e-j) use the right colorbar. (k-n) The contribution of BVOC, soil NO_x (SNO_x), BVOC together with soil NO_x (BVOC+SNO_x) for a north (36.0-42.0°N, 105.0-117.5°E) and south (26.0-32.0°N, 107.5-120.0°E) region (purple and black boxes in (a) and (b)).